Invariant-EKF design for quadcopter wind estimation

Hao Chen[1] He Bai[1] Clark N. Taylor[2]

***Abstract*— We consider a nonlinear estimation problem where a quadcopter moves in a wind field. We show that the quadcopter dynamics is invariant under the action of a Lie group and design an Invariant Extended Kalman Filter (IEKF) by taking advantage of symmetry in the system dynamics. The IEKF estimates the quadcopter's position, velocity, orientation and wind velocity using measured position, acceleration, magnetic field, angular velocity, and control thrust. The resulting design is implemented and validated in simulations. Through Monte-Carlo (MC) simulations, we demonstrate that the IEKF produces improved transient estimation performance over a conventional Extended Kalman Filter (EKF) for a variety of wind fields.**

I. INTRODUCTION

Wind estimation techniques for small unmanned aerial vehicles (sUAV) have received increasing attention in the past few years. There are mainly two motivations. First, wind estimation can improve navigation performance of sUAV and further improve their flight performance. Because of sUAV small sizes and limited propulsion power, they are sensitive to wind gusts which may cause unstable or even unsafe flight, especially in the situations requiring sUAV to avoid obstacles [1]. The second motivation is mainly from environmental studies and meteorology, where sUAV are used for atmospheric measurements (see e.g., [2]). The traditional and common atmospheric observation platforms, like towers or tethered balloons, are expensive, labor intensive and hard to operate [3]. sUAV provide an alternative platform for atmospheric research and data collection because they are low cost and easy to operate.

While much prior research has emphasized the development of fixed-wing UAV for atmospheric investigations [4], the use of multi-rotor aircraft is relatively less explored. A fixed-wing UAV typically flies horizontally for some distance and it cannot hover at one point in space. By comparison, a rotary-wing UAV (RUAV) does not have the above limitations and can therefore be used to estimate vertical wind profiles or temporal variability of the wind at one point.

There are four major approaches for RUAV wind estimation:

1) **Mounting sensors on multi-rotors**. In [5], [6], the authors use the RUAV equipped with different types of anemometers to estimate wind field. However, this approach may reduce flight endurance due to the weight and power requirements of sensors and the platform. Obtaining the inertial measurement of the wind may be difficult in strong winds since the motion of quadcopter in this case is not null [7]. In addition, accurate and reliable wind sensors are typically expensive compared with an sUAV platform.

2) **Static mapping methods**. Ross et al. in [3] find a linear relation between the squared wind speed and the tilt angle through anemometer-collected wind speed data and show effectiveness of the wind estimation by using the above relation. The authors in [8] and [9] explore the relation of the tilt and the air-relative velocity, and calculate the wind vector using the air-relative vector and the measured ground vector using the wind triangle. However, this method has shown effectiveness only in slight wind fields.

3) **Machine learning methods**. Reference [10] trains a long short-term memory neural network (LSTM NN) on roll and pitch angles and quadcopter positions based on data generated from a simulated quadcopter in turbulent wind fields. In [11], two machine learning methods, K-nearest neighbor (KNN) and LSTM, are used to estimate the wind velocity and turbulence characterization from real attitude measurements. The LSTM outperforms the KNN and the linear model method under variable wind conditions. Machine learning approaches can learn the wind-attitude relationship directly from the available data, so it does not require a mathematical model. However, these approaches may require high quality training data and estimate the wind vector without considering uncertainty in the sUAV states. Machine learning results may be specific to the training data of a RUAV quadcopter and unable to extend other RUAVs.

4) **Model-based methods**. Model-based methods have been proposed to estimate both the vehicle's states and the wind field. The study in [12] uses an EKF to estimate the wind based on a linearized-about-hover dynamic particle model and shows an improvement compared to methods that use a static relation between tilt and wind. Reference [13] improves the above method and uses the EKF to estimate the wind based on a nonlinear dynamic model. Animesh et al. in [14] develop a self-calibration framework for the online state, parameter and wind field estimation based on square-root unscented Kalman filter. A model-based filter can be integrated with existing autopilots to improve navigation and control performance.

In this paper, we take the model-based approach and explore an invariant extended Kalman filter (IEKF) design to estimate both the quadcopter states and the wind. Invariant filters take advantage of symmetry properties inherent in the system dynamics to appropriately choose the estimation

[1]H. Chen and H. Bai are with Mechanical and Aerospace Engineering, Oklahoma State University, Stillwater, OK 74078, USA. he.bai@okstate.edu, hao.chen@okstate.edu

[2]C. N. Taylor is with the Department of Electrical and Computer Engineering, Air Force Institute of Technology, Wright-Patterson, OH, USA. clark.taylor@afit.edu.

The work of the first two authors is supported by the National Science Foundation (NSF) under Grant No. 1925147

error coordinates. Bonnabel et al. [15] introduce invariant observers that leverages symmetries of nonlinear systems to improve estimation performance. The authors in [16] and [17] also illustrate good performance of symmetry-preserving observers for state estimation.

When the gain matrix in an invariant observer is determined by the EKF approach, the resulting EKF is an invariant EKF (IEKF) [18], [19]. IEKF has become popular in localization, navigation and sensor fusion for robotic systems. A generalized multiplicative EKF and a discrete EKF on Lie groups are developed in [20] and [21], respectively. Reference [22] shows that the IEKF in a deterministic context has good local convergence properties for a well characterized class of systems. The authors in [23] derive an IKEF on matrix lie groups. Reference [24] designs IEKFs with additive disturbances and proposes a correction to IEKF covariances to better represent uncertainties. Recently, the relation between invariant system, group affine system and equivariant system is studied and a new filter design using equivariance of the system is proposed in [25].

Our IEKF is designed to estimate a quadcopter's position, velocity, orientation and wind velocity based on measurements from a GPS, an Inertial Measurement Unit (IMU), a magnetometer and thrust measurements. We first identify the invariance properties in the dynamics when there is wind. We then derive an invariant observer and determine its gain based on the invariant error dynamics. We conduct Monte-Carlo simulations for hover and non-hover tests in different wind fields, including a constant wind field, turbulent wind fields generated from a Large Eddy Simulation (LES) at two different altitudes and a sinusoidal wind field.

The main contribution of this paper is the design of an IEKF that fuses thrust, GPS, IMU and magnetometer measurements to estimate state and wind information for a quadcopter. We also explore its performance compared with a conventional EKF and identify where the IEKF outperforms the EKF in the simulations with various types of wind fields. Our results show that the IEKF produces faster convergence and smaller overshoot in the transient performance compared to an EKF.

The rest of the paper is organized as follows. In Section II, we introduce our quadcopter system dynamics with the drag force and measurement equations. In Section III, we present the invariance property of the system dynamics and equaivariance of the measurements, and in Section IV, we derive our IEKF algorithm. Section V provides simulation results for hover tests and non-hover tests under different wind fields. Conclusions and future work are presented in Section VI.

II. Problem Formulation

The translational dynamics and attitude kinematics of a quadcopter subject to a wind disturbance in the north-east-down (NED) frame can be represented as:

$$\begin{aligned} \dot{x} &= R_b v \\ m\dot{v} &= mv \times \omega + mR_b^T \boldsymbol{g} + \boldsymbol{f}_c + f_{\text{drag}} + mR_b^T \dot{v}_w \\ \dot{R}_b &= R_b S(\omega) \end{aligned} \tag{1}$$

where $x \in \mathbb{R}^3$ is the inertial position, $v \in \mathbb{R}^3$ is the ground velocity in the body frame, $v_w \in \mathbb{R}^3$ is the wind velocity in the inertial frame, $R_b \in SO(3)$ is the orientation of the quadcopter with respect to the inertial frame, $\boldsymbol{g} = [0,0,g]^T \in \mathbb{R}^3$ denotes the gravity acceleration vector in inertial frame, $\boldsymbol{f_c} = [0,0,-f_c]^T \in \mathbb{R}^3$ denotes the thrust vector in body frame where f_c is the amplitude of the thrust control input, f_{drag} denotes the drag force due to air resistance (described with more details below) and $\omega \in \mathbb{R}^3$ is the angular velocity in the body frame. The function $S(\cdot) : \mathbb{R}^3 \to so(3)$ satisfies $S(a)b = a \times b$ for $a, b \in \mathbb{R}^3$.

We assume that the wind velocity v_w is the output of a linear dynamics system

$$\dot{d} = Ad, \quad v_w = Cd, \tag{2}$$

where $d \in \mathbb{R}^{m\times 1}$, $A \in \mathbb{R}^{m\times m}$, $C \in \mathbb{R}^{3\times m}$ and the matrices A and C are assumed known. Such wind dynamics can be used to model various types of mean wind profiles, such as sinusoidal and constant wind. In filter implementation, we add process noise to the d dynamics to mitigate the effect of the turbulent component in the wind.

Denote by $v_r \in \mathbb{R}^3$ the relative air velocity in the body frame. That is, $v_r = v - R_b^T v_w$. The drag force f_{drag} is modeled as a function of v_r

$$f_{\text{drag}} = f(v_r) = -\frac{1}{2}\rho D |v_r| v_r, \;\; D = \begin{pmatrix} D_x & 0 & 0 \\ 0 & D_y & 0 \\ 0 & 0 & D_z \end{pmatrix}, \tag{3}$$

where ρ is the air density and D denotes the drag coefficient matrix. The D_x and D_y are usually the same but different from D_z due to the geometry of a quadcopter [7]. Such a model is adapted from a classic 1-D drag model $f_{\text{drag}} = 1/2\rho S v_r^2$ [10].

Using the wind dynamics in (2) and the drag force in (3), we rewrite the dynamics in (1) in terms of x, v_r, R_b and d as

$$\begin{aligned} \dot{x} &= R_b v_r + Cd \\ \dot{v}_r &= v_r \times \omega + R_b^T \boldsymbol{g} + \frac{1}{m}\boldsymbol{f}_c + \frac{1}{m} f_{\text{drag}} \\ \dot{R}_b &= R_b S(\omega) \\ \dot{d} &= Ad \end{aligned} \tag{4}$$

We further define the state as $X = (x, v_r, R_b, d)$ and the input as $U = (\omega, \boldsymbol{f}_c, D)$. The input U is used to build invariance of system dynamics in the next section. Therefore, it can include constant parameters of the system, such as the D matrix.

We assume that the quadcopter is equipped with a GPS, a 3-axis accelerometer and gyroscope, and a magnetometer. We assume that biases of the sensors are calibrated. The measured angular velocity from the gyroscope and thrust

control vector ($\boldsymbol{f_c}$) are used in the system dynamics as inputs. The measured outputs $y = (y_x^T, y_a^T, y_b^T)^T$ are

$$y = h(X,U) = \begin{pmatrix} x \\ a \\ R_b^T B \end{pmatrix}, a = \frac{1}{m}\left(\boldsymbol{f_c} + f_{\text{drag}}\right) \tag{5}$$

where $B \in \mathbb{R}^3$ is the earth's magnetic field expressed in the inertial frame and $a \in R^3$ is the specific acceleration vector in the body frame.

Given the system dynamics with the drag force (3) and the measurement model (5), we next investigate symmetry properties in the dynamics, based on which we can design invariant filters to estimate both the wind field and the quadcopter states.

III. Invariance of the Dynamics and Equivariance of the Measurements

The symmetries of the system are associated with the Euclidean group $G = SE(3)$ which consists of rotations and translations in dimension 3. Let $(x_g, R_g) \in G$, where $x_g \in \mathbb{R}^3$ and $R_g \in SO(3)$. The subscript g in here denotes (x_g, R_g) is the element of the group instead of gravity coefficient. Define two transformations on the state X and the input U as

$$\varphi_g(X) = \begin{pmatrix} x + x_g \\ R_g v_r \\ R_b R_g^T \\ d \end{pmatrix}, \psi_g(U) = \begin{pmatrix} R_g \omega \\ R_g \boldsymbol{f_c} \\ R_g D R_g^T \end{pmatrix}. \tag{6}$$

Proposition 1. *The system (4) is invariant with respect to the transformations $\varphi_g(X)$ and $\psi_g(U)$. The measurement equation* (5) *is G-equivariant.*

Proof: According to definition 2 in [15], the system is said to be invariant for all g, X, U if

$$\frac{d}{dt}(\varphi_g(X)) = f(\varphi_g(X), \psi_g(U)). \tag{7}$$

By setting $\varphi_g(X) = [\tilde{x}, \tilde{v}_r, \tilde{R}_b, \tilde{d}]$ and $\psi_g(U) = [\tilde{\omega}, \tilde{\boldsymbol{f}}_c, \tilde{D}]$, we verify

$$\begin{aligned}
\dot{\tilde{x}} &= \dot{x} + \dot{x}_g = R_b v_r + Cd = R_b R_g^T R_g v_r + C\tilde{d} \\
&= \tilde{R}_g \tilde{v}_r + C\tilde{d}, \\
\dot{\tilde{v}}_r &= R_g \dot{v}_r = R_g(v_r \times \omega + R_b^T \boldsymbol{g} + \frac{1}{m}\boldsymbol{f}_c + \frac{1}{m}(-\frac{1}{2}\rho D|v_r|v_r)) \\
&= R_g v_r \times R_g \omega + R_g R_b^T \boldsymbol{g} + \frac{1}{m} R_g \boldsymbol{f_c} \\
&+ \frac{1}{m}(-\frac{1}{2}\rho R_g D R_g^T |R_g v_r| R_g v_r) \\
&= \tilde{v}_r \times \tilde{\omega} + \tilde{R}_b^T \boldsymbol{g} + \frac{1}{m}\tilde{\boldsymbol{f}}_c + \frac{1}{m} f(\tilde{v}_r), \\
\dot{\tilde{R}}_b &= \dot{R}_b R_g^T = R_b S(\omega) R_g^T = R_b R_g^T R_g S(\omega) R_g^T = \tilde{R}_b S(\tilde{\omega}), \\
\dot{\tilde{d}} &= \dot{d} = A\tilde{d}.
\end{aligned}$$

Since the dynamics of the transformed variables shown above satisfies (7), (4) is invariant under the transformation (6).

Similarly, the measurement equation is G-equivariant if there exists a $\varrho_g(\cdot)$ such that

$$\varrho_g(h(X,U)) = h(\varphi_g(X), \psi_g(U)). \tag{8}$$

We define

$$\varrho_g(h(X,U)) = \begin{pmatrix} x + x_g \\ R_g a \\ R_g R_b^T B \end{pmatrix} = \begin{pmatrix} x + x_g \\ R_g \frac{1}{m}(\boldsymbol{f}_c - \frac{1}{2}\rho D|v_r|v_r) \\ R_g R_b^T B \end{pmatrix} \tag{9}$$

and verify

$$\begin{aligned}
h(\varphi_g(X), \psi_g(U)) &= \begin{pmatrix} \tilde{x} \\ \frac{1}{m}(\tilde{\boldsymbol{f}}_c - \frac{1}{2}\rho\tilde{D}|\tilde{v}_r|\tilde{v}_r) \\ \tilde{R}_b^T B \end{pmatrix} \\
&= \begin{pmatrix} x + x_g \\ R_g \frac{1}{m}(\boldsymbol{f}_c - \frac{1}{2}\rho D|v_r|v_r) \\ R_g R_b^T B \end{pmatrix}.
\end{aligned} \tag{10}$$

Since $\varrho_g(y(X,U)) = y(\varphi_g(X), \psi_g(U))$, the measurement equation (5) is G-equivariant. □

It is straightforward to use the same transformations and show the same invariance property for a linear drag of the form $f_{\text{drag}} = Dv_r$ [26]. Similar system dynamics of a flying rigid body without the drag term has been shown invariant in [16]. Our work introduces the transformation on D and extends the existing result to show that the dynamics are invariant under wind disturbances with arbitrary linear wind dynamics and quadratic drag model.

IV. IEKF Design

Using the invariance property in Proposition 1, we next design an invariant estimator based on the unit quaternion representation of R_b. We employ the design method outlined in [15].

A. Invariant observer

Let $q \in \mathbb{R}^4$ be the unit quaternion representing R_b. The system dynamics (4) becomes

$$\begin{aligned}
\dot{x} &= q * v_r * q^{-1} + Cd \\
\dot{v}_r &= v_r \times \omega + q^{-1} * \boldsymbol{g} * q + \frac{1}{m}\boldsymbol{f}_c + \frac{1}{m} f(v_r) \\
\dot{q} &= \frac{1}{2} q * \omega \\
\dot{d} &= Ad
\end{aligned} \tag{11}$$

where $*$ denotes the quaternion multiplication. In a quaternion multiplication, any vector in $\mathbb{R}^3$ is augmented to a quaternion with 0 being the scalar part.

1) Invariants and invariant output error: We split $\varphi_g(X)$ into $\varphi_g^a(X)$ and $\varphi_g^b(X)$ such that $\varphi_g^a(X)$ is invertible with respect to g. The implicit function theorem ensures the existence of the local solution $g = \gamma$. The normalization equation is

$$\varphi_\gamma^a(X) = \begin{pmatrix} x + x_\gamma \\ q * q_\gamma^{-1} \end{pmatrix} = \begin{pmatrix} 0 \\ 1 \end{pmatrix} \tag{12}$$

where 1 is the unit quaternion. Hence,

$$\gamma(X) = \begin{pmatrix} x_\gamma \\ q_\gamma \end{pmatrix} = \begin{pmatrix} -x \\ q \end{pmatrix}. \tag{13}$$

Let $\hat{X}$ be an estimate of X. We now solve for the invariants using $I = (\varphi^b_{\gamma(\hat{X})}(\hat{X}), \psi_{\gamma(\hat{X})}(U))$, where

$$\varphi^b_{\gamma(\hat{X})}(\hat{X}) = \begin{pmatrix} \hat{q} * \hat{v}_r * \hat{q}^{-1} \\ \hat{d} \end{pmatrix}, \psi_{\gamma(\hat{X})}(U) = \begin{pmatrix} \hat{q} * \boldsymbol{\omega} * \hat{q}^{-1} \\ \hat{q} * \boldsymbol{f}_c * \hat{q}^{-1} \\ R(\hat{q}) D R^T(\hat{q}) \end{pmatrix}. \tag{14}$$

Therefore, the invariants are

$$\begin{aligned} I =& (I_{v_r}, I_d, I_\omega, I_{\boldsymbol{f}_c}, I_D) \\ =& (\hat{q} * \hat{v}_r * \hat{q}^{-1}, \hat{d}, \hat{q} * \boldsymbol{\omega} * \hat{q}^{-1}, \hat{q} * \boldsymbol{f}_c * \hat{q}^{-1}, R(\hat{q}) D R^T(\hat{q})). \end{aligned} \tag{15}$$

The invariant output error is given by

$$\begin{aligned} E =& \varrho_{\gamma(\hat{X})}(y) - \varrho_{\gamma(\hat{X})}(\hat{y}) \\ =& \begin{pmatrix} x - \hat{x} \\ \hat{q} * (a - \hat{a}) * \hat{q}^{-1} \\ \hat{q} * (y_b - \hat{y}_b) * \hat{q}^{-1} \end{pmatrix} = T \begin{pmatrix} y_x - \hat{y}_x \\ y_a - \hat{y}_a \\ y_b - \hat{y}_b \end{pmatrix} = \begin{pmatrix} E_x \\ E_a \\ E_b \end{pmatrix}, \end{aligned} \tag{16}$$

where T is given below with e_i, $i = 1,2,3$, forming the canonical frame of $\mathbb{R}^3$:

$$T = \begin{pmatrix} e_i & 0 & 0 \\ 0 & \hat{q} * e_i * \hat{q}^{-1} & 0 \\ 0 & 0 & \hat{q} * e_i * \hat{q}^{-1} \end{pmatrix}. \tag{17}$$

2) Invariant frame: The invariant frame is given by

$$W = (D\varphi_{\gamma(X)}(X))^{-1} \frac{\partial}{\partial X} = \begin{pmatrix} e_i & 0 & 0 & 0 \\ 0 & \hat{q}^{-1} * e_i * \hat{q} & 0 & 0 \\ 0 & 0 & e_i * \hat{q} & 0 \\ 0 & 0 & 0 & e_i \end{pmatrix}. \tag{18}$$

3) Invariant pre-observer: The invariant pre-observer is designed as follows

$$\begin{aligned} \dot{\hat{x}} &= \hat{q} * \hat{v}_r * \hat{q}^{-1} + C\hat{d} + \bar{\mathcal{L}}^x E \\ \dot{\hat{v}}_r &= \hat{v}_r \times \boldsymbol{\omega} + \hat{q}^{-1} * \boldsymbol{g} * \hat{q} + \frac{1}{m} \boldsymbol{f}_c + \frac{1}{m} f(\hat{v}_r) \\ &\quad + \hat{q}^{-1} * (\bar{\mathcal{L}}^{v_r} E) * \hat{q} \\ \dot{\hat{q}} &= \frac{1}{2} \hat{q} * \boldsymbol{\omega} + (\bar{\mathcal{L}}^q E) * \hat{q} \\ \dot{\hat{d}} &= A\hat{d} + \bar{\mathcal{L}}^d E, \end{aligned} \tag{19}$$

where $\bar{\mathcal{L}}^\star$ is the gain matrix

$$\bar{\mathcal{L}}^\star \in \mathbb{R}^{3\times 9}, \quad \star \in \{x, v_r, q, d\}. \tag{20}$$

4) Dynamics of invariant error: The invariant state error is given by $\eta = \varphi_{\gamma(\hat{X})}(X) - \varphi_{\gamma(\hat{X})}(\hat{X}) = [\eta_x \ \ \eta_{v_r} \ \ \eta_q \ \ \eta_d]^T$. We next differentiate η with respect to time and obtain the invariant error dynamics

$$\begin{aligned} \dot{\eta}_x &= \eta_q * \eta_{v_r} * \eta_q^{-1} + \eta_q * I_{v_r} * \eta_q^{-1} + C\eta_d - I_{v_r} - \bar{\mathcal{L}}^x E \\ \dot{\eta}_{v_r} &= \eta_q^{-1} * \boldsymbol{g} * \eta_q - \boldsymbol{g} + \frac{1}{m}(-\frac{1}{2}\rho I_D |I_{vr} + \eta_{vr}|(I_{vr} + \eta_{vr})) \\ &\quad - \frac{1}{m}(-\frac{1}{2}\rho I_D |I_{vr}| I_{vr}) + (\bar{\mathcal{L}}^q E) * \eta_{v_r} - \bar{\mathcal{L}}^{v_r} E \\ \dot{\eta}_q &= -\eta_q * (\bar{\mathcal{L}}^q E) \\ \dot{\eta}_d &= A\eta_d - (\bar{\mathcal{L}}^d E). \end{aligned} \tag{21}$$

Linearizing above invariant error dynamics and invariant output E around $\eta_x = 0, \eta_{v_r} = 0, \eta_q = [1,0,0,0]^T, \eta_d = 0$ yields the state matrix A_k and output matrix H_k needed for implementing the IEKF:

$$A_k = \begin{pmatrix} 0 & I_3 & 0 & -2S(I_{v_r}) & C \\ 0 & \alpha & 0 & 2S(\boldsymbol{g}) & 0 \\ 0 & 0 & 0 & 0 & 0 \\ 0 & 0 & 0 & 0 & A \end{pmatrix}, \tag{22}$$

$$H_k = \begin{pmatrix} I_3 & 0 & 0 & 0 \\ 0 & \alpha & 0 & 0 \\ 0 & 0 & 2S(B) & 0 \end{pmatrix}, \tag{23}$$

where I_3 is the 3 by 3 identity matrix and $\alpha = \frac{1}{m}(-\frac{1}{2}\rho I_D)\frac{\partial |I_{vr} + \eta_{vr}|(I_{vr} + \eta_{vr})}{\partial \eta_{vr}}$.

B. IEKF Algorithm

To derive the IEKF algorithm, the process noise $w = [w_x^T, w_\omega^T, w_f, w_d^T]^T$ is added to the invariant observer (19). The IEKF algorithm employs (19) with $L = 0$ and the linearized matrix A_k in (22) to propagate the estimates and the covariance between measurement updates. For the correction step, we select L as the Kalman filter gain based on A_k and H_k and update $\hat{X}$ using L and the measurements $y_m = (y_{x_m}^T, y_{a_m}^T, y_{b_m}^T)^T$. We note that the invariant state error rotates the conventional estimation error to another frame. To represent the uncertainty more accurately, the initial state covariance and process noise and measurement noise covariance matrices, P_0, Q, and R, need to be transformed to the invariant frame from the original frame [22], [24]. The transformed matrices are given by: $P_{0_{rot}} = W^T P_0 W$, $Q_{rot} = NQN^T$, and $R_{rot} = TRT^T$ where $N = \frac{\partial \dot{\eta}}{\partial w}$ and $\dot{\eta}$ is the invariant error dynamics (21) with process noise, T and W are given in (17) and (18), respectively. The IEKF algorithm is given in Algorithm 1.

Algorithm 1: The proposed IEKF

Initialize X_0, P_0 in the original coordinates.
$P = W^T P_0 W$
for $k = 1$ **to** n **do**
  Prediction: in between measurements $(t \in [t_{k-1}, t_k])$
  Propagate $\dot{\hat{X}} = f(\hat{X}, U)$ according to (19) with $L = 0$ to get $\hat{X}_k^-$
  Compute A_k from (22)
  Compute $Q_{rot} = NQN^T$
  Propagate $\dot{P} = A_k P + P A_k^T + Q_{rot}$ to get P_k^-
  Correction: at the k^{th} **sensor measurement** $(t = t_k)$
  $R_{rot} = TRT^T$
  Compute H_k from (22)
  $L_k = P_k^- H_k^T (H_k P_k^- H_k^T + R_{rot})^{-1}$
  $\hat{X}_k^+ = \hat{X}_k^- + W L_k T(y_{m,k} - h(\hat{X}_k^-, U))$
  $P_k^+ = (I - L_k H_k) P_k^-$
end

V. Simulations

In this section, we conduct Monte-Carlo simulations and compare the estimation performance of the EKF and the designed IEKF under hover and non-hover tests for different wind fields. The first one is the constant wind equal to $(3,2,0)^T$ m/s. The second and third wind fields are generated from large eddy simulations (LES) [27] capturing the low-altitude turbulence effect. In Fig. 1, we show the LES wind at 8 and 50 meters in altitude at 1Hz, respectively. The fourth wind is a sinusoidal wind. Due to the page limit, we only present the simulation results for the LES wind at 8 meters in the hover test.

We construct a Simulink quadcopter model which consists of sensor models, a motor model, a rotor model and the quadcopter rigid body dynamics. Details of the model can be found in Section II.A of [10]. A feedback linearization attitude controller and a PID position controller are used for the quadcopter model. The thrust measurements used in the filters are calculated from the control inputs obtained form the attitude controller. The parameters of the quadcopter and the sensor parameters are given in Table I.

TABLE I
System Parameters

Name	Symbol	Value	Units
mass	m	1.5	kg
x moment of inertia	J_x	0.0348	$kg \cdot m^2$
y moment of inertia	J_y	0.0459	$kg \cdot m^2$
z moment of inertia	J_z	0.0977	$kg \cdot m^2$
x body drag coeff.	D_x	0.3265	kg/m
y body drag coeff.	D_y	0.3265	kg/m
z body drag coeff.	D_z	0.3265*2	kg/m
air density	ρ	1.225	kg/m^3
GPS noise SD	σ_{gps}	1	m
accel noise SD	σ_{accel}	$0.0025g$	m/s^2
gyro noise SD	σ_{gyro}	0.0023	rad/s
mag noise SD	σ_{mag}	1	mG
GPS frequency	f_{gps}	1	Hz
accel frequency	f_{accel}	100	Hz
gyro frequency	f_{gyro}	100	Hz
mag frequency	f_{mag}	100	Hz
true magnetic field		$[200,-40,480]$	mG

We conduct Monte Carlo simulations of 50 runs. For the hover test, the quadcopter flies from a random starting point which is around the origin to a goal point and then hovers at that point. For non-hover tests, the quadcopter flies a square trajectory. Each simulation lasts for 100 seconds.

The following parameters are used in all the simulations: $\mu_0 = [0,0,0,0,0,0,1,0,0,0,0,0,0]^T$, $P_0 = diag(1,1,1,1,1,1,0,0.004^2,0.005^2,0.044^2,1,1,0.1)$, $X_0 \sim N(\mu_0, P_0)$ and $\hat{X}_0 = \mu_0$. where X_0 represents the true initial states used in quadcopter model and $\hat{X}_0$ represents the initial states for the EKF and the IEKF. The process noise and measurement noise covariance matrices under the constant wind are

$$Q = diag(0,0,0,0.0023^2,0.0023^2,0.0023^2,0,0,0,0)$$
$$R = diag(1,1,1,0.025^2,0.025^2,0.025^2,1,1,1).$$

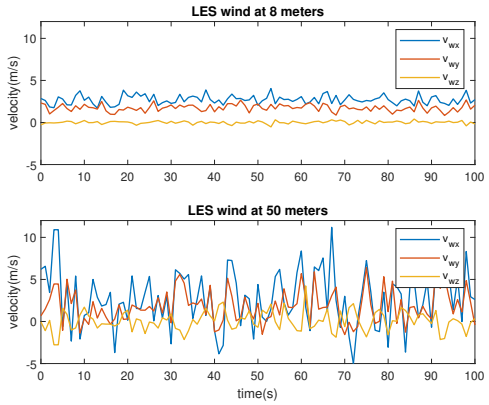

Fig. 1. LES wind fields at 8 and 50 meters in altitude, respectively. The wind data is generated at 1Hz.

where Q corresponds to the process noise w. Because the LES wind at 8 meters and 50 meters contains turbulence, the last three diagonal elements of the Q matrix are adjusted to $[0.01^2,0.01^2,0.01^2]$ and $[0.1^2,0.1^2,0.1^2]$, respectively. For hover and LES wind case, the A and C matrices used in the filter are $A = 0_{3\times3}$ and $C = diag(1,1,1)$.

The wind estimation results from one run of the MC simulations under the four different wind fields all show IEKF outperform EKF at transient part. For example, as shown in Fig. 2 for LES wind (8m) test, the estimated wind of the IEKF has a much smaller error at the beginning and converges more quickly compared to the wind estimation of the EKF.

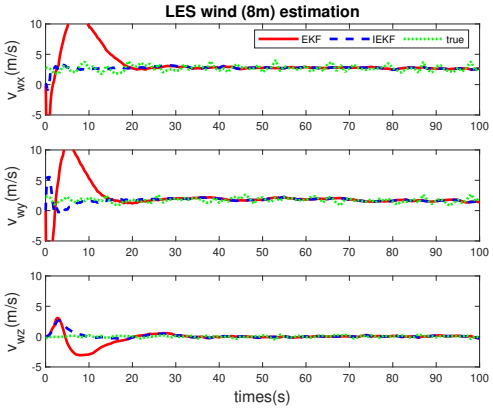

Fig. 2. Comparison of the IEKF and the EKF wind estimation for a single run using LES wind at 8 meters in the hover test.

The RMSEs of the IEKF and the EKF show a similar trend for the four different wind fields under hover and non-hover tests. In Fig. 3, we show the RMSEs of the estimation performance of position x, $v_{r,x}$, yaw angle and $v_{w,x}$ between the EKF and the IEKF for the first 30 seconds. Since the RMSE of the EKF has a large spike at the beginning compared to that of the IEKF, we choose reasonable ranges for the y axis of four plots in Fig. 3. RMSEs of the EKF have large errors and converge more slowly, especially for position and wind.

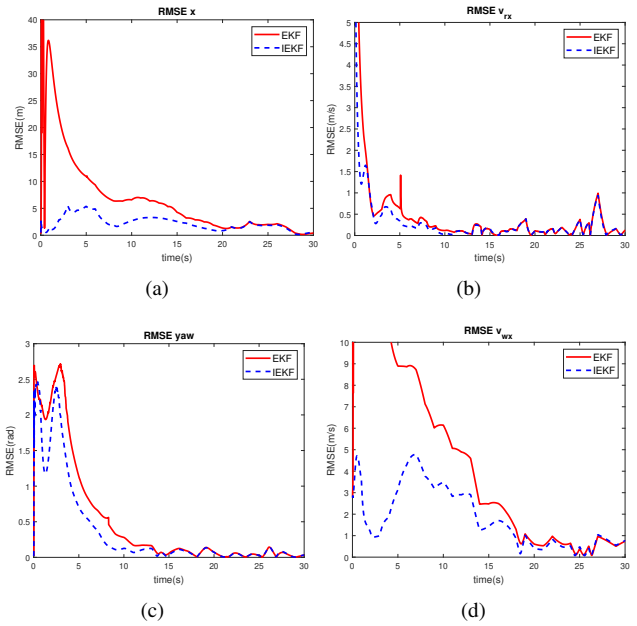

Fig. 3. RMSE comparison of the EKF and the IEKF under LES wind at 8 meters in the hover test. (a): RMSE of the position x estimate. (b): RMSE of v_{rx} estimate. (c): RMSE of yaw angle estimate. (d): RMSE of v_{wx} estimate.

VI. Conclusions and Future Work

In this paper, we investigate simultaneous state and wind estimation for a quadcopter dynamics under wind disturbances. We establish the invariance of the system dynamics augmented with linear wind dynamics and the equivariance of the measurement equation under the proposed Lie group actions. We design an IEKF estimator and conduct simulations to validate its performance. Our results demonstrate that the IEKF produces better transient estimation performance compared to a conventional EKF for various wind fields.

The designed IEKF relies on knowledge of the drag model. Future work includes examining robustness of the IEKF against uncertainties in the drag models, addressing biases in IMU measurements, and experimental validation on a quadcopter platform.

References

[1] B. Arain and F. Kendoul, "Real-time wind speed estimation and compensation for improved flight," *IEEE Transactions on Aerospace and Electronic Systems*, vol. 50, no. 2, pp. 1599–1606, 2014.

[2] J. D. Jacob, P. B. Chilson, A. L. Houston, and S. W. Smith, "Considerations for atmospheric measurements with small unmanned aircraft systems," *Atmosphere*, vol. 9, no. 7, p. 252, 2018.

[3] R. T. Palomaki, N. T. Rose, M. van den Bossche, T. J. Sherman, and S. F. De Wekker, "Wind estimation in the lower atmosphere using multirotor aircraft," *Journal of Atmospheric and Oceanic Technology*, vol. 34, no. 5, pp. 1183–1191, 2017.

[4] P. Tian, H. Chao, M. Rhudy, J. Gross, and H. Wu, "Wind sensing and estimation using small fixed-wing unmanned aerial vehicles: A survey," *Journal of Aerospace Information Systems*, pp. 1–12, 2021.

[5] I. De Boisblanc, N. Dodbele, L. Kussmann, R. Mukherji, D. Chestnut, S. Phelps, G. C. Lewin, and S. de Wekker, "Designing a hexacopter for the collection of atmospheric flow data," in *2014 Systems and Information Engineering Design Symposium (SIEDS)*. IEEE, 2014, pp. 147–152.

[6] C. A. Wolf, R. P. Hardis, S. D. Woodrum, R. S. Galan, H. S. Wichelt, M. C. Metzger, N. Bezzo, G. C. Lewin, and S. F. de Wekker, "Wind data collection techniques on a multi-rotor platform," in *2017 Systems and Information Engineering Design Symposium (SIEDS)*. IEEE, 2017, pp. 32–37.

[7] J. González-Rocha, C. A. Woolsey, C. Sultan, and S. F. De Wekker, "Sensing wind from quadrotor motion," *Journal of Guidance, Control, and Dynamics*, vol. 42, no. 4, pp. 836–852, 2019.

[8] P. P. Neumann and M. Bartholmai, "Real-time wind estimation on a micro unmanned aerial vehicle using its inertial measurement unit," *Sensors and Actuators A: Physical*, vol. 235, pp. 300–310, 2015.

[9] C. Brosy, K. Krampf, M. Zeeman, B. Wolf, W. Junkermann, K. Schäfer, S. Emeis, and H. Kunstmann, "Simultaneous multicopter-based air sampling and sensing of meteorological variables," *Atmospheric Measurement Techniques*, vol. 10, no. 8, pp. 2773–2784, 2017.

[10] S. Allison, H. Bai, and B. Jayaraman, "Wind estimation using quadcopter motion: A machine learning approach," *Aerospace Science and Technology*, vol. 98, p. 105699, 2020.

[11] D. Crowe, R. Pamula, H. Y. Cheung, and S. F. De Wekker, "Two supervised machine learning approaches for wind velocity estimation using multi-rotor copter attitude measurements," *Sensors*, vol. 20, no. 19, p. 5638, 2020.

[12] J. Moyano Cano, "Quadrotor UAV for wind profile characterization," Master's thesis, 2013.

[13] V. S. Pappu, Y. Liu, J. F. Horn, and J. Cooper, "Wind gust estimation on a small VTOL UAV," in *Proceedings of the 7th AHS Technical Meeting on VTOL Unmanned Aircraft Systems and Autonomy, Mesa, AZ, USA*, 2017, pp. 24–26.

[14] A. Shastry and D. Paley, "UAV state and parameter estimation in wind using calibration trajectories optimized for observability," *IEEE Control Systems Letters*, 2020.

[15] S. Bonnabel, P. Martin, and P. Rouchon, "Symmetry-preserving observers," *IEEE Transactions on Automatic Control*, vol. 53, no. 11, pp. 2514–2526, 2008.

[16] P. Martin and E. Salaun, "A general symmetry-preserving observer for aided attitude heading reference systems," in *2008 47th IEEE Conference on Decision and Control*. IEEE, 2008, pp. 2294–2301.

[17] M. Barczyk and A. F. Lynch, "Invariant extended kalman filter design for a magnetometer-plus-gps aided inertial navigation system," in *2011 50th IEEE Conference on Decision and Control and European Control Conference*. IEEE, 2011, pp. 5389–5394.

[18] S. Bonnabel, "Left-invariant extended kalman filter and attitude estimation," in *2007 46th IEEE Conference on Decision and Control*. IEEE, 2007, pp. 1027–1032.

[19] S. Bonnable, P. Martin, and E. Salaün, "Invariant extended kalman filter: theory and application to a velocity-aided attitude estimation problem," in *Proceedings of the 48h IEEE Conference on Decision and Control (CDC) held jointly with 2009 28th Chinese Control Conference*. IEEE, 2009, pp. 1297–1304.

[20] P. Martin and E. Salaün, "Generalized multiplicative extended kalman filter for aided attitude and heading reference system," in *AIAA Guidance, Navigation, and Control Conference*, 2010, p. 8300.

[21] G. Bourmaud, R. Mégret, A. Giremus, and Y. Berthoumieu, "Discrete extended kalman filter on lie groups," in *21st European Signal Processing Conference (EUSIPCO 2013)*. IEEE, 2013, pp. 1–5.

[22] A. Barrau and S. Bonnabel, "The invariant extended kalman filter as a stable observer," *IEEE Transactions on Automatic Control*, vol. 62, no. 4, pp. 1797–1812, 2016.

[23] K. S. Phogat and D. E. Chang, "Invariant extended kalman filter on matrix lie groups," *Automatica*, vol. 114, p. 108812, 2020.

[24] K. Coleman, H. Bai, and C. N. Taylor, "Extended invariant-EKF designs for state and additive disturbance estimation," *Automatica*, vol. 125, p. 109464, 2021.

[25] R. Mahony and J. Trumpf, "Equivariant filter design for kinematic systems on lie groups," *IFAC-PapersOnLine*, vol. 54, no. 9, pp. 253–260, 2021.

[26] J. Svacha, K. Mohta, and V. Kumar, "Improving quadrotor trajectory tracking by compensating for aerodynamic effects," in *2017 international conference on unmanned aircraft systems (ICUAS)*. IEEE, 2017, pp. 860–866.

[27] R. K. S. S. Vuppala and K. Kara, "Large-eddy simulation of atmospheric boundary-layer gusts for small unmanned air systems," *Bulletin of the American Physical Society*, 2020.